Femtosecond laser micromachining of lithium niobate depressed cladding waveguides

Ruiyun He,[1] Qiang An,[1] Yuechen Jia,[1] Gabriel R. Castillo-Vega, [2] Javier R. Vázquez de Aldana,[2] and Feng Chen[1,*]

[1]*School of Physics, State Key Laboratory of Crystal Materials and Key Laboratory of Particle Physics and Particle Irradiation, Ministry of Education, Shandong University, Jinan 250100, China*
[2]*Laser Microprocessing Group, Universidad de Salamanca, Salamanca 37008, Spain*
[*]*drfchen@sdu.edu.cn*

Abstract: We report on the fabrication and characterization of femtosecond laser micromachined depressed cladding waveguides in lithium niobate crystal. The cladding structures support two-dimensional guidance of light from the visible to the mid-infrared spectral regimes. Particularly, single-mode propagation of light at a wavelength of 4 μm has been achieved for the waveguides with diameter of 50 μm. It is also found that the thermal annealing treatment reduces the propagation loss lower than 0.5 dB/cm at 1.064 μm, exhibiting good transmission properties for photonic applications.

©2013 Optical Society of America

OCIS codes: (140.3390) Laser materials processing; (230.7370) Waveguides; (160.3730) Lithium niobate.

References and links

1. E. J. Murphy, *Integrated Optical Circuits and Components: Design and Applications* (Marcel Dekker, 1999).
2. C. Grivas, "Optically pumped planar waveguide lasers, Part I: Fundamentals and fabrication techniques," Prog. Quantum Electron. **35**(6), 159–239 (2011).
3. D. Jaque, E. Cantelar, and G. Lifante, "Lattice micro-modifications induced by Zn diffusion in Nd:LiNbO$_3$ channel waveguides probed by Nd^{3+} confocal micro-luminescence," Appl. Phys. B **88**(2), 201–204 (2007).
4. F. Chen, "Micro-and submicrometric waveguiding structures in optical crystals produced by ion beams for photonic applications," Laser Photon. Rev. **6**(5), 622–640 (2012).
5. A. Tervonen, B. R. West, and S. Honkanen, "Ion-exchanged glass waveguide technology: a review," Opt. Eng. **50**(7), 071107 (2011).
6. K. M. Davis, K. Miura, N. Sugimoto, and K. Hirao, "Writing waveguides in glass with a femtosecond laser," Opt. Lett. **21**(21), 1729–1731 (1996).
7. S. Juodkazis, V. Mizeikis, and H. Misawa, "Three-dimensional microfabrication of materials by femtosecond laser for photonics applications," J. Appl. Phys. **106**(5), 051101 (2009).
8. Y. Liao, J. Song, E. Li, Y. Luo, Y. Shen, D. Chen, Y. Cheng, Z. Xu, K. Sugioka, and K. Midorikawa, "Rapid prototyping of three-dimensional microfluidic mixers in glass by femtosecond laser direct writing," Lab Chip **12**(4), 746–749 (2012).
9. L. B. Fletcher, J. J. Witcher, N. Troy, S. T. Reis, R. K. Brow, and D. M. Krol, "Direct femtosecond laser waveguide writing inside zinc phosphate glass," Opt. Express **19**(9), 7929–7936 (2011).
10. A. Okhrimchuk, V. Mezentsev, A. Shestakov, and I. Bennion, "Low loss depressed cladding waveguide inscribed in YAG:Nd single crystal by femtosecond laser pulses," Opt. Express **20**(4), 3832–3843 (2012).
11. G. A. Torchia, A. Rodenas, A. Benayas, E. Cantelar, L. Roso, and D. Jaque, "Highly efficient laser action in femtosecond-written Nd:yttrium aluminum garnet ceramic waveguides," Appl. Phys. Lett. **92**(11), 111103 (2008).
12. F. Chen and J. R. Vázquez de Aldana, "Optical waveguides in crystalline dielectric materials produced by femtosecond-laser micromachining," Laser Photonics Rev. DOI 10.1002/lpor.201300025.
13. H. L. Liu, Y. C. Jia, J. R. Vázquez de Aldana, D. Jaque, and F. Chen, "Femtosecond laser inscribed cladding waveguides in Nd:YAG ceramics: Fabrication, fluorescence imaging and laser performance," Opt. Express **20**(17), 18620–18629 (2012).
14. Y. Y. Ren, G. Brown, A. Ródenas, S. Beecher, F. Chen, and A. K. Kar, "Mid-infrared waveguide lasers in rare-earth-doped YAG," Opt. Lett. **37**(16), 3339–3341 (2012).
15. H. Hu, R. Ricken, W. Sohler, and R. B. Wehrspohn, "Lithium niobate ridge waveguides fabricated by wet etching," IEEE Photon. Technol. Lett. **19**(6), 417–419 (2007).
16. F. Chen, "Photonic guiding structures in lithium niobate crystals produced by energetic ion beams," J. Appl. Phys. **106**(8), 081101 (2009).

17. E. M. Rodríguez, D. Jaque, E. Cantelar, F. Cussó, G. Lifante, A. C. Busacca, A. Cino, and S. R. Sanseverino, "Time resolved confocal luminescence investigations on reverse proton exchange Nd:LiNbO$_3$ channel waveguides," Opt. Express **15**(14), 8805–8811 (2007).

18. A. Ródenas, A. H. Nejadmalayeri, D. Jaque, and P. Herman, "Confocal Raman imaging of optical waveguides in LiNbO$_3$ fabricated by ultrafast high-repetition rate laser-writing," Opt. Express **16**(18), 13979–13989 (2008).

19. J. Thomas, M. Heinrich, P. Zeil, V. Hilbert, K. Rademaker, R. Riedel, S. Ringleb, C. Dubs, J. Ruske, S. Nolte, and A. Tünnermann, "Laser direct writing: Enabling monolithic and hybrid integrated solutions on the lithium niobate platform," Phys. Status Solidi A **208**(2), 276–283 (2011).

20. J. Burghoff, S. Nolte, and A. Tünnermann, "Origins of waveguiding in femtosecond laser-structured LiNbO$_3$," Appl. Phys., A Mater. Sci. Process. **89**(1), 127–132 (2007).

21. M. Heinrich, A. Szameit, F. Dreisow, S. Döring, J. Thomas, S. Nolte, A. Tünnermann, and A. Ancona, "Evanescent coupling in arrays of type II femtosecond laser-written waveguides in bulk x-cut lithium niobate," Appl. Phys. Lett. **93**(10), 101111 (2008).

22. Y. Liao, J. Xu, Y. Cheng, Z. Zhou, F. He, H. Sun, J. Song, X. Wang, Z. Xu, K. Sugioka, and K. Midorikawa, "Electro-optic integration of embedded electrodes and waveguides in LiNbO$_3$ using a femtosecond laser," Opt. Lett. **33**(19), 2281–2283 (2008).

23. H. T. Bookey, R. R. Thomson, N. D. Psaila, A. K. Kar, N. Chiodo, R. Osellame, and G. Cerullo, "Femtosecond laser inscription of low insertion loss waveguides in Z-cut lithium niobate," IEEE Photon. Technol. Lett. **19**(12), 892–894 (2007).

24. B. H. Lee, E. C. Wood, M. S. Zahniser, J. B. McManus, D. D. Nelson, S. C. Herndon, G. W. Santoni, S. C. Wofsy, and J. W. Munger, "Simultaneous measurements of atmospheric HONO and NO$_2$ via absorption spectroscopy using tunable mid-infrared continuous-wave quantum cascade lasers," Appl. Phys. B **102**(2), 417–423 (2011).

25. M. Skorczakowski, J. Swiderski, W. Pichola, P. Nyga, A. Zajac, M. Maciejewska, L. Galecki, J. Kasprzak, S. Gross, A. Heinrich, and T. Bragagna, "Mid-infrared Q-switched Er:YAG laser for medical applications," Laser Phys. Lett. **7**(7), 498–504 (2010).

26. S. Mirov, V. Fedorov, I. Moskalev, D. Martyshkin, and C. Kim, "Progress in Cr^{2+} and Fe^{2+} doped mid-IR laser materials," Laser Photon. Rev. **4**(1), 21–41 (2010).

27. H. C. Guo, S. H. Tang, Z. D. Gao, Y. Q. Qin, S. N. Zhu, and Y. Y. Zhu, "Multiple-channel mid-infrared optical parametric oscillator in periodically poled MgO:LiNbO$_3$," J. Appl. Phys. **101**(11), 113112 (2007).

28. C. Heese, C. R. Phillips, L. Gallmann, M. M. Fejer, and U. Keller, "Ultrabroadband, highly flexible amplifier for ultrashort midinfrared laser pulses based on aperiodically poled Mg:LiNbO$_3$," Opt. Lett. **35**(14), 2340–2342 (2010).

29. G. Z. Mashanovich, M. M. Milošević, M. Nedeljkovic, N. Owens, B. Xiong, E. J. Teo, and Y. Hu, "Low loss silicon waveguides for the mid-infrared," Opt. Express **19**(8), 7112–7119 (2011).

30. A. J. Maker and A. M. Armani, "Low-loss silica-on-silicon waveguides," Opt. Lett. **36**(19), 3729–3731 (2011).

31. A. Ródenas, G. Martin, B. Arezki, N. Psaila, G. Jose, A. Jha, L. Labadie, P. Kern, A. Kar, and R. Thomson, "Three-dimensional mid-infrared photonic circuits in chalcogenide glass," Opt. Lett. **37**(3), 392–394 (2012).

32. J. Siebenmorgen, K. Petermann, G. Huber, K. Rademaker, S. Nolte, and A. Tunnermann, "Femtosecond laser written stress-induced Nd:Y$_3$Al$_5$O$_{12}$ (Nd:YAG) channel waveguide laser," Appl. Phys. B **97**(2), 251–255 (2009).

33. RSoft Design Group, Computer software BandSLOVE, http://www.rsoftdesign.com

34. D. Yevick and W. Bardyszewski, "Correspondence of variational finite-difference (relaxation) and imaginary-distance propagation methods for modal analysis," Opt. Lett. **17**(5), 329–330 (1992).

1. Introduction

Optical waveguides, as the basic components in integrated photonics, offer the confinement of light propagation within small volumes, in which relatively high optical intensities could be achieved [1,2]. Many techniques (e.g., thermal ion in-diffusion, ion implantation/irradiation, ion/proton exchange and femtosecond (fs) laser micromachining/writing) have been employed to fabricate waveguide structures in various materials [3–6]. As one of the most efficient techniques for direct three dimensional (3D) microfabrication of transparent materials [7,8], fs-laser micromachining has been utilized to fabricate optical waveguides in various materials, including glasses, crystals, ceramics [9–14], etc. By using the fs laser micromachining, three configurations of waveguides could be fabricated: Type I directly written waveguides, Type II stress-induced waveguides, and Type III depressed cladding waveguides [12]. In most crystals, the fs laser beams generate negative refractive index changes in the irradiated tracks. In this way, Type II structures (typically with dual line geometry) are popular owing to the stress induced effect. Recently, depressed cladding waveguides attract much attention as well, due to some of the emerging advantages. In most crystals, cladding waveguides may support nearly balanced guidance along TE and TM polarizations [13]. More importantly, the flexible diameters and shapes of the waveguide

cross sections make depressed cladding waveguides feasible to construct the fiber-waveguide integrated photonic chips, supporting guidance till longer wavelength regimes [14].

Lithium niobate (LiNbO$_3$) is one of the most widely applied nonlinear and electro-optic crystals. As of yet, a number of LiNbO$_3$ waveguides of different morphologies, mechanisms and performances have been fabricated by using various techniques [15–19]. Fs-laser micromachined waveguides of Type I and II geometries have been realized in LiNbO$_3$ crystals [19–23]. However, to the best of our knowledge, depressed cladding waveguides in LiNbO$_3$ crystal have not been reported.

On the other hand, the mid-infrared (MIR) wavelength range is a spectral region of a number of scientific and technological interests. The two atmospheric transmission windows of 3-5 μm and 8-13 μm, in which the earth's atmosphere is relatively transparent, are important for widely applications, such as atmospheric, chemical and medical [24,25]. With the emergence of new generations of MIR laser sources, the MIR part of the spectra has become a region of increased emphasis in recent years [26]. Many optical devices in LiNbO$_3$ crystals have been investigated in MIR band [27,28]. In the aspect of optical waveguides, MIR waveguides have been realized in YAG crystal [14], silicon-on-insulator [29], silica on silicon [30], and chalcogenide glass [31], etc. Therefore, the production of depressed cladding waveguides in LiNbO$_3$ crystal and investigation of the guiding characteristics at MIR wavelength regime remain meaningful goals yet to be solved.

In this work, we report on the depressed cladding waveguides in LiNbO$_3$ crystal produced by fs-laser micromachining. Guiding properties of the cladding waveguides are investigated under laser sources with wavelengths ranging from visible to MIR bands.
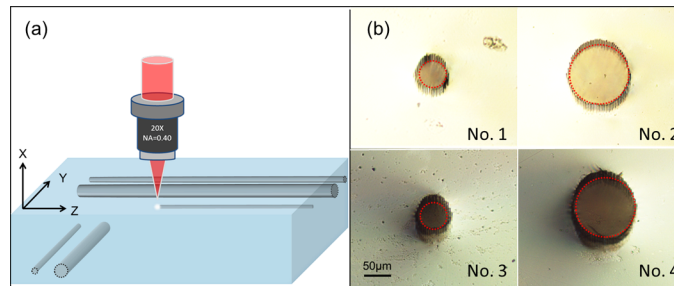
2. Experiments

Fig. 1. (a) Schematic of the depressed cladding waveguides preparation. (b) Optical microscope images of the cross sections of the LiNbO$_3$ depressed cladding waveguides Nos. 1-4. The red dashed circles indicate the locations of the cladding waveguides.

The LiNbO$_3$ crystal was cut to 1 (x) × 10(y) × 10(z) mm^3 with all its surfaces optically polished. An amplified Ti:Sapphire laser system, which produced pulses of 120 fs duration, 1 mJ maximum pulse energy at a repetition of 1 kHz and linearly polarized at 800 nm, was utilized to fabricate cladding waveguides in LiNbO$_3$ crystal. The precise value of the pulse energy was controlled with a calibrated neutral density filter, a half-wave plate and a linear polarizer. The sample was located at a three-axis motorized stage which could move with the setting velocity and direction. In order to fabricate the cladding waveguides, a large set of parallel damage tracks have to be inscribed in the crystal at different depths of the sample, following a circular geometry with the desired diameter. To this end, the laser beam was focused through one of the largest sample surfaces (dimensions 10 × 10 mm^2) at a maximum depth of ~150 μm by a 20 × microscope objective (N.A. = 0.40). The scanning velocity was set to a relatively high speed of 0.5 mm/s (to minimize the stress effect induced by the fs laser pulses) and the separation between neighboring damage tracks was 3 μm. Two waveguides with diameters 50 and 110 μm (No. 1 and No. 2 respectively) were fabricated by scanning the sample along the z axis with pulse energy of 2.1 μJ. Another two claddings with the same diameters (No. 3 and No. 4) were produced by focusing the laser beam beneath the opposite

surface with pulse energy of 5.04 μJ and scanning the sample along the *y* axis of crystal. A schematic of depressed cladding waveguides preparation is depicted in Fig. 1(a).

The microscope images of the cladding waveguide cross sections were taken by using an optical microscope (Axio Imager, Carl Zeiss) operating in transmission mode. The near field modal distributions were investigated by utilizing a typical end-face arrangement. Microscope objective lenses or convex lenses were used to couple the light into and out of the waveguides. The wavelength from visible to MIR of the laser sources (i.e., a He-Ne laser at 633-nm, a solid state laser at 1064 nm (MIL-III1064, CNI Optoelectronics Co. Ltd), and a tunable laser at 4 μm (MIRTM 8025, Daylight Solutions Inc.)). A CCD camera (CinCam, CINOGY Technologies) was used to record the data at 0.633 μm and 1.064 μm. In MIR spectrum, we used a 2-16 μm beam imaging camera (WinCamD, DataRay Inc.). Based on the end-face arrangement, the N.A. of the cladding waveguides were measured to estimate the maximum refractive index changes of the cladding waveguides at 0.633 μm, 1.064 μm and 4 μm, respectively. Insertion losses of the $LiNbO_3$ depressed cladding waveguides at each wavelength were also estimated. A thermal annealing at 260 °C for 1 hour at open air was employed to improve the waveguides qualities.

3. Results and discussion

Figure 1(b) shows the optical microscope images of the cross sections of the $LiNbO_3$ depressed cladding waveguides Nos. 1-4. As one can see, the cladding waveguide cores, as identified by the red dashed circles, were located in the regions surrounded by the fs-laser inscribed tracks.
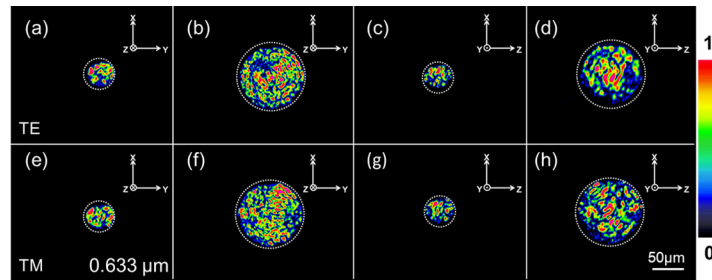

Fig. 2. The near field modal distributions of $LiNbO_3$ cladding waveguides (a) and (e) No. 1, (b) and (f) No. 2, (c) and (g) No. 3, (d) and (h) No. 4 for the TE (top) and TM (bottom) polarizations at 0.633 μm. The dashed circles indicate the spatial locations of the boundaries of the waveguide structures.
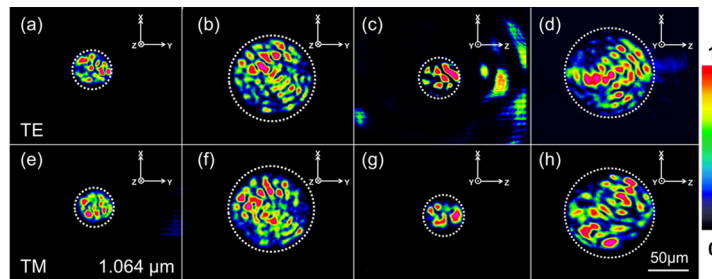

Fig. 3. The near field modal distributions of $LiNbO_3$ cladding waveguides (a) and (e) No. 1, (b) and (f) No. 2, (c) and (g) No. 3, (d) and (h) No. 4 for the TE (top) and TM (bottom) polarizations at 1.064 μm. The dashed circles indicate the spatial locations of the boundaries of the waveguide structures.

The $LiNbO_3$ cladding waveguides support two-dimensional (2D) light transmission along both polarizations from the visible to the mid-infrared wavelength regimes. Figures 2-4 depict the measured near field modal distributions of the $LiNbO_3$ depressed cladding waveguides at wavelengths of 0.633, 1.064 and 4 μm, respectively. The crystalline orientations are also

indicated. In these three figures, the modal distributions in (c) and (d) were along the extraordinary index (n_e) polarization, while the others were along the ordinary index (n_o) polarization. As one can see, the near field modal distributions at 0.633 μm and 1.064 μm were highly multimode, which were in agreement with the theoretical estimation from the guided-wave optics. It is clear from Fig. 4. that waveguides No. 1 and No. 3 were single-mode along both polarizations at 4 μm. Waveguides No. 2 and No. 4 (both with diameter of 110 μm) showed multimode guiding up to 4 μm, which implies the potential for effective guiding in the whole MIR transmission range of LiNbO₃ up to 5.5 μm wavelength. In previous works on LiNbO₃, Type I waveguides showed guidance only along the n_e polarization [19, 20]. Type II waveguides in LiNbO₃ crystal support guidance along both polarizations, however, it was weak for the n_o polarization [20]. As one can see, the 2D guidance of the depressed cladding waveguides fabricated in this work shows a better performance.
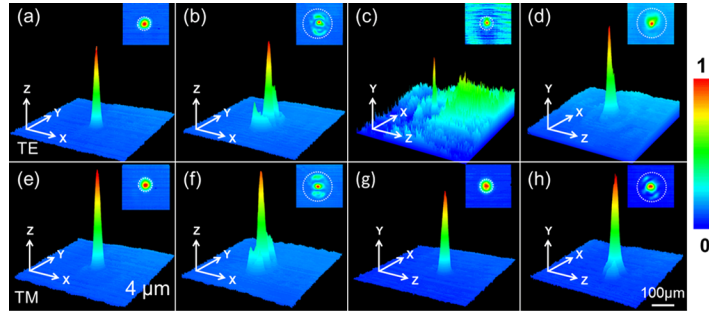

Fig. 4. 2D, 3D measured near field modal distributions of LiNbO₃ cladding waveguides: (a) and (e) No. 1, (b) and (f) No. 2, (c) and (g) No. 3, (d) and (h) No. 4 for the TE (top) and TM (bottom) polarizations at 4 μm. The dashed lines in the insets indicate the spatial locations of the boundaries of the waveguides.

In order to reconstruct the 2D refractive index profile of the LiNbO₃ depressed cladding waveguides, we first assumed that the distribution was a step-like one based on the numerical aperture method [32]. By measuring the maximum incident angle θ_m at which no change of the transmitted power was occurring, the refractive index contrasts between the low-index damage filaments and the waveguide core region were roughly estimated with the Eq. (1),

$$\Delta n \approx \frac{\sin^2 \theta_m}{2n} \qquad (1)$$

Where n was the refractive index of the bulk at the corresponding wavelength. In this work, the calculated maximum refractive index contrasts were 4.1×10^{-3} and 5.1×10^{-3} for waveguides No. 1 and No. 2 along both polarizations at 4 μm, respectively. However, for waveguides No. 3 and No. 4, the values of the n_e polarization were 1.6×10^{-3} and 3.1×10^{-3}, which were smaller than that of n_o polarization (i.e. 3.4×10^{-3} and 4.9×10^{-3}). The disadvantage of smaller refractive index alternations may lead to the poor guiding properties along n_e polarization, which could obviously be drawn from Figs. 4(c) and 4(d), as well as the insertion losses discussed below.
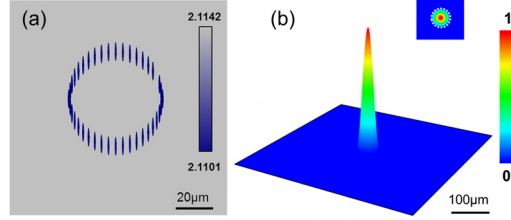
Fig. 5. (a) Reconstructed 2D refractive index profile and (b) 2D, 3D calculated near field modal distributions of the LiNbO$_3$ cladding waveguide No. 1.

With the obtained Δn, one can reconstruct the 2D refractive index profile of the LiNbO$_3$ cladding waveguides. Since the profiles are similar, we simply exhibit the one of waveguide No.1 for brevity. Figure 5(a) shows the reconstructed 2D refractive index profile at the cross section of cladding waveguide No. 1 at 4 μm. Based on the reconstructed 2D refractive index profile, we simulated the light propagation at that wavelength by using the software Rsoft©, which based on the finite difference beam propagation method (FD-BPM) [33,34]. Figure 5(b) shows the calculated modal distributions of LiNbO$_3$ cladding waveguide No. 1. By comparing Fig. 4(a) with Fig. 5(b), one can see that the calculated profiles are in good agreement with the experimental results, which proves that the reconstructed refractive index profile of the waveguide is reasonable.

Based on the end-face arrangement, we measured the insertion losses α (including propagation loss and coupling loss but excluding the Fresnel reflection in the interface of the waveguide end face and the air) of the LiNbO$_3$ cladding waveguides, as shown in Table 1. Data at different wavelengths from visible to MIR basically follow the same law. According to the values of the insertion losses, it showed $\alpha_3 > \alpha_4$ and $\alpha_1 > \alpha_2$ along both polarizations, that is to say cladding waveguides with diameter of 110 μm showed superior guiding performance to those of 50 μm. However, the insertion losses of waveguides No. 3 and No. 4 along n_e polarization were larger than the values measured along n_o polarization, leading to $\alpha_3 > \alpha_4 > \alpha_1 > \alpha_2$ along TE polarization, and $\alpha_3 > \alpha_1 > \alpha_4 > \alpha_2$ for the TM polarization.

After annealing, the insertion losses reduced as shown in Table 1. In particular, in the 10 mm long waveguide with minimum insertion losses (No. 2) they were decreased to 1.0 dB, 0.5 dB and 3.0 dB at 0.633 μm, 1.064 μm and 4 μm, respectively. In previous works, the propagation losses reported for Type II waveguides in LiNbO$_3$ were 1 dB/cm [22], 4 dB/cm [21] at 633 nm and 0.6 dB/cm [20] at 1.064 μm. A minimum insertion loss of 3.5 dB at 1550 nm was measured for the 18 mm long Type I LiNbO$_3$ waveguide [23]. The results for the cladding waveguides represent comparable or even better transmission properties to those from the reported fs-laser written waveguides in LiNbO$_3$ crystal.

Table 1. Insertion losses α (dB) of the LiNbO$_3$ cladding waveguides

Waveguide	TE/TM	α (dB) before annealing			α (dB) after annealing		
		0.633 μm	1.064 μm	4 μm	0.633 μm	1.064 μm	4 μm
No. 1	TE	3.2	2.2	4.9	2.7	1.7	4.3
	TM	3.4	2.3	5.0	2.9	1.6	4.3
No. 2	TE	1.2	1.5	4.4	1.0	0.5	3.0
	TM	1.2	1.6	4.3	1.0	0.5	3.0
No. 3	TE	10.2	7.3	12.7	7.1	3.3	12.4
	TM	7.4	3.9	5.9	3.6	2.6	5.0
No. 4	TE	7.0	3.4	8.6	5.2	2.0	7.1
	TM	3.0	1.7	4.9	1.8	0.8	3.7

4. Summary

We have fabricated cladding waveguides in LiNbO$_3$ crystal by using fs-laser micromachining. The cladding structures with diameter of 50 μm and 110 μm support guidance along both n_e and n_o polarizations at wavelengths of 0.633 μm, 1.064 μm and 4 μm. At the wavelength of 4 μm, single modes are achieved for the cladding waveguides with diameter of 50 μm. The

minimum loss was reduced to 0.5 dB/cm after thermal annealing. The good transmission properties suggest promising applications of LiNbO$_3$ guiding devices in integrated photonics.